Cell

# Allosteric Inhibition of the IRE1α RNase Preserves Cell Viability and Function during Endoplasmic Reticulum Stress

Rajarshi Ghosh,[1,2,5,6,7,12] Likun Wang,[1,5,6,7,12] Eric S. Wang,[2,12] B. Gayani K. Perera,[8] Aeid Igbaria,[1,5,6,7] Shuhei Morita,[1,5,6,7] Kris Prado,[1,5,6,7] Maike Thamsen,[1,5,6,7] Deborah Caswell,[2] Hector Macias,[1,5] Kurt F. Weiberth,[1,5,6,7] Micah J. Gliedt,[1,6] Marcel V. Alavi,[3] Sanjay B. Hari,[8] Arinjay K. Mitra,[8] Barun Bhhatarai,[10] Stephan C. Schürer,[9,10] Erik L. Snapp,[11] Douglas B. Gould,[3,4] Michael S. German,[1,5] Bradley J. Backes,[1,6] Dustin J. Maly,[8] Scott A. Oakes,[2,5,*] and Feroz R. Papa[1,5,6,7,*]
[1]Department of Medicine
[2]Department of Pathology
[3]Department of Ophthalmology
[4]Department of Anatomy
[5]Diabetes Center
[6]Lung Biology Center
[7]California Institute for Quantitative Biosciences
University of California, San Francisco, San Francisco, CA 94143, USA
[8]Department of Chemistry, University of Washington, Seattle, WA 98195, USA
[9]Center for Computational Science
[10]Department of Molecular and Cellular Pharmacology,
Miller School of Medicine, University of Miami, FL 33136, USA
[11]Department of Anatomy and Structural Biology, Albert Einstein College of Medicine, Bronx, NY 10461, USA
[12]Co-first author
*Correspondence: scott.oakes@ucsf.edu (S.A.O.), frpapa@medicine.ucsf.edu (F.R.P.)
http://dx.doi.org/10.1016/j.cell.2014.07.002

## SUMMARY

Depending on endoplasmic reticulum (ER) stress levels, the ER transmembrane multidomain protein IRE1α promotes either adaptation or apoptosis. Unfolded ER proteins cause IRE1α lumenal domain homo-oligomerization, inducing *trans* autophosphorylation that further drives homo-oligomerization of its cytosolic kinase/endoribonuclease (RNase) domains to activate mRNA splicing of adaptive XBP1 transcription factor. However, under high/chronic ER stress, IRE1α surpasses an oligomerization threshold that expands RNase substrate repertoire to many ER-localized mRNAs, leading to apoptosis. To modulate these effects, we developed ATP-competitive IRE1α *K*inase-*I*nhibiting *R*Nase *A*ttenuators—KIRAs—that allosterically inhibit IRE1α's RNase by breaking oligomers. One optimized KIRA, KIRA6, inhibits IRE1α in vivo and promotes cell survival under ER stress. Intravitreally, KIRA6 preserves photoreceptor functional viability in rat models of ER stress-induced retinal degeneration. Systemically, KIRA6 preserves pancreatic β cells, increases insulin, and reduces hyperglycemia in Akita diabetic mice. Thus, IRE1α powerfully controls cell fate but can itself be controlled with small molecules to reduce cell degeneration.

## INTRODUCTION

Secreted and transmembrane proteins fold and assemble in the endoplasmic reticulum (ER) through reactions catalyzed by ER-resident activities. When these reactions are saturated or corrupted, cells experience "ER stress," and unfolded protein accumulation in the ER triggers intracellular signaling pathways termed the unfolded protein response (UPR). The UPR induces transcription of genes encoding ER chaperones, oxidoreductases, and ER-associated degradation (ERAD) components (Travers et al., 2000), while inhibiting translation (Harding et al., 2000). These outputs are adaptive because they enhance ER protein-folding capacity, reduce secretory protein load, and promote degradation of ER unfolded proteins.

However, if ER stress remains irremediably high and adaptive outputs are overwhelmed, alternative "terminal UPR" signals trigger apoptosis. Although cell death under high ER stress may protect organisms from exposure to improperly folded secretory proteins, many human degenerative diseases, such as diabetes mellitus and retinopathies, may be caused by excessive ER stress-induced cell death (Shore et al., 2011). Mechanistic understanding of critical terminal UPR signaling events may lead to effective therapies for such conditions.

Unfolded ER proteins activate three ER transmembrane sensors—PERK, ATF6, and IRE1α—by changing their oligomerization state in the ER membrane (Kohno, 2007). IRE1α, the most ancient of these components, senses unfolded proteins either directly or indirectly through an ER lumenal domain that

becomes oligomerized during stress (Credle et al., 2005; Zhou et al., 2006). Subsequently, IRE1α's bifunctional kinase/endoribonuclease (RNase) activities become juxtaposed on its cytosolic face, allowing monomers to *trans*-autophosphorylate. Kinase autophosphorylation conformationally activates IRE1α's RNase to site-specifically cleave the XBP1 mRNA. Religation and translation of XBP1 mRNA in an alternate open reading frame produces the XBP1s transcription factor, whose targets encode proteins that enhance ER protein folding and quality control (Calfon et al., 2002; Lee et al., 2003; Yoshida et al., 2001). Thus, IRE1α promotes adaptation via XBP1s.

However, under high ER stress, IRE1α's RNase relaxes its substrate specificity to endonucleolytically cleave many other mRNAs that localize to the ER membrane as their encoded proteins undergo cotranslational translocation (Han et al., 2009; Hollien et al., 2009). IRE1α's RNase also cleaves precursors of apoptosis-inhibitory microRNAs (Lerner et al., 2012; Upton et al., 2012).

Here, we show that multiple terminal UPR outputs, including cell proliferation blocks, sterile inflammation, and apoptosis result from kinase-driven increases in the oligomerization state of IRE1α's cytosolic domains that hyperactivate its RNase. These destructive events are prevented by breaking IRE1α oligomerization through rational mutations or somatic mutations found in the *Ire1α* gene of various human cancers. To test physiological effects of pharmacologically inhibiting IRE1α, we developed small-molecule kinase inhibitors that prevent oligomerization and allosterically inhibit its RNase. One such IRE1α kinase inhibitor preserves viability and function in ER-stressed cells, pancreatic islet explants, and rodent models of ER stress-induced retinitis pigmentosa and diabetes.

## RESULTS

### IRE1α's Kinase Is a Rheostat that Employs Self-Association to Control RNase Activity

Previously, we proposed that IRE1α's kinase regulates catalytic activity of its adjoining RNase in a graduated manner to impact cell fate in mammals, yet the mechanistic basis for the rheostatic control remained unclear (Han et al., 2009). Here, we hypothesized that the degree of self-association of kinase/RNase subunits on the cytosolic face connects IRE1α phosphorylation status to RNase activation levels. Increasing phosphorylation of the IRE1α kinase may proportionally increase the oligomeric state of kinase/RNase subunits past a critical threshold, thereby driving RNase activity into a hyperactive state. Consequently, IRE1α RNase expands its specificity past its canonical XBP1 mRNA substrate, endonucleolytically cleaving many ER-localized mRNAs and pushing cells into apoptosis. In this view, IRE1α's lumenal domains are responsive to protein-folding conditions in the ER, but rheostatic control by the kinase over the RNase ultimately determines cell fate. If these predictions are correct, genetic and small-molecule control over IRE1α kinase oligomerization should enable cell fate control, irrespective of upstream ER stress.

To begin testing this hypothesis, we employed IRE1α recombinant proteins and cell lines. Artificial ER stress agents are widely used to acutely activate the UPR, but saturating doses that have no natural pathophysiological correlate are often employed. To test cytoprotection later in the work, we established dose-response regimes using three ER stress agents that dose-dependently push rat insulinoma (INS-1) cells, which have a well-developed ER and secrete insulin, past a stress threshold and, in switch-like manner, into apoptosis. The percentage of INS-1 cells entering apoptosis due to the ER $Ca^{2+}$ pump inhibitor thapsigargin (Tg) depends aggregately on two variables: concentration and duration of exposure (Figures S1A and S1B available online). Similar results hold for the glycosylation inhibitor tunicamycin (Tm) and the anterograde trafficking inhibitor brefeldin A (BFA) (Figures S1C and S1D). Preceding apoptosis, increasing ER stress agent levels progressively increase IRE1α phosphorylation, XBP1 mRNA splicing, endonucleolytic decay of the ER-localized mRNA, Ins1 mRNA (which encodes proinsulin), induction of thioredoxin-interacting protein (TXNIP) mRNA (whose product activates the NLRP3 inflammasome), and downstream c-Jun terminal kinase (JNK) phosphorylation (Figures S1E and S1F).

All of these terminal UPR signature events, culminating in apoptosis, can be simulated, without imposing ER stress, by conditionally overexpressing wild-type (WT) IRE1α in INS-1 stable lines (Han et al., 2009). Induced with doxycycline (Dox), the transgenic IRE1α (WT) proteins spontaneously self-associate, *trans*-autophosphorylate, and trigger XBP1 mRNA splicing (Figures 1A and 1B) (Han et al., 2009). Increasing [Dox] causes progressive decay of Ins1 mRNA, elevation of TXNIP mRNA, and apoptosis (Figures 1C and 1D). Thus, as with ER stress agents, dose escalation of transgenic IRE1α (WT) allows graduated control over the terminal UPR and is sufficient to push cells, in switch-like manner, into apoptosis (Figure 1E).

To study how IRE1α autophosphorylation impacts oligomeric state and RNase substrate selectivity, we expressed and purified a recombinant soluble miniprotein—called IRE1α*—containing the kinase/RNase domains. Salt bridges formed through phosphoamino groups in neighboring IRE1α kinases contribute to kinase/RNase homo-oligomerization (Ali et al., 2011; Korennykh et al., 2009). IRE1α* is basally autophosphorylated and spontaneously homo-oligomerizes as its concentration is raised (Figures 1F and 1G). Dephosphorylation of IRE1α* with λ-phosphatase—dP-IRE1α*—reduces the oligomer/monomer ratio, confirming that phosphorylation drives oligomerization.

We next tested the impact of IRE1α* oligomerization on RNase activity against in-vitro-transcribed XBP1 RNA and a less efficient substrate, Ins2 RNA, derived from one of the two mRNA isoforms encoding rodent proinsulin (Figures 1H and 1I). We also utilized an IRE1α* variant whose oligomeric state can be controlled with a small molecule. Mutation of IRE1α* at the isoleucine (I) gatekeeper residue to glycine (G) in its kinase ATP-binding pocket creates a "hole"—IRE1α* (I642G); in the full-length protein, the I642G mutation cripples autophosphorylation (Han et al., 2009). As with dP-IRE1α*, IRE1α* (I642G) has reduced oligomerization compared to IRE1α* (Figures 1F and 1G). 1NM-PP1 is a "bumped" kinase inhibitor that selectively binds mutant kinases that contain glycine gatekeeper residues. Working as a ligand, 1NM-PP1 increases IRE1α* (I642G) oligomerization but to levels well below those of equimolar IRE1α*.

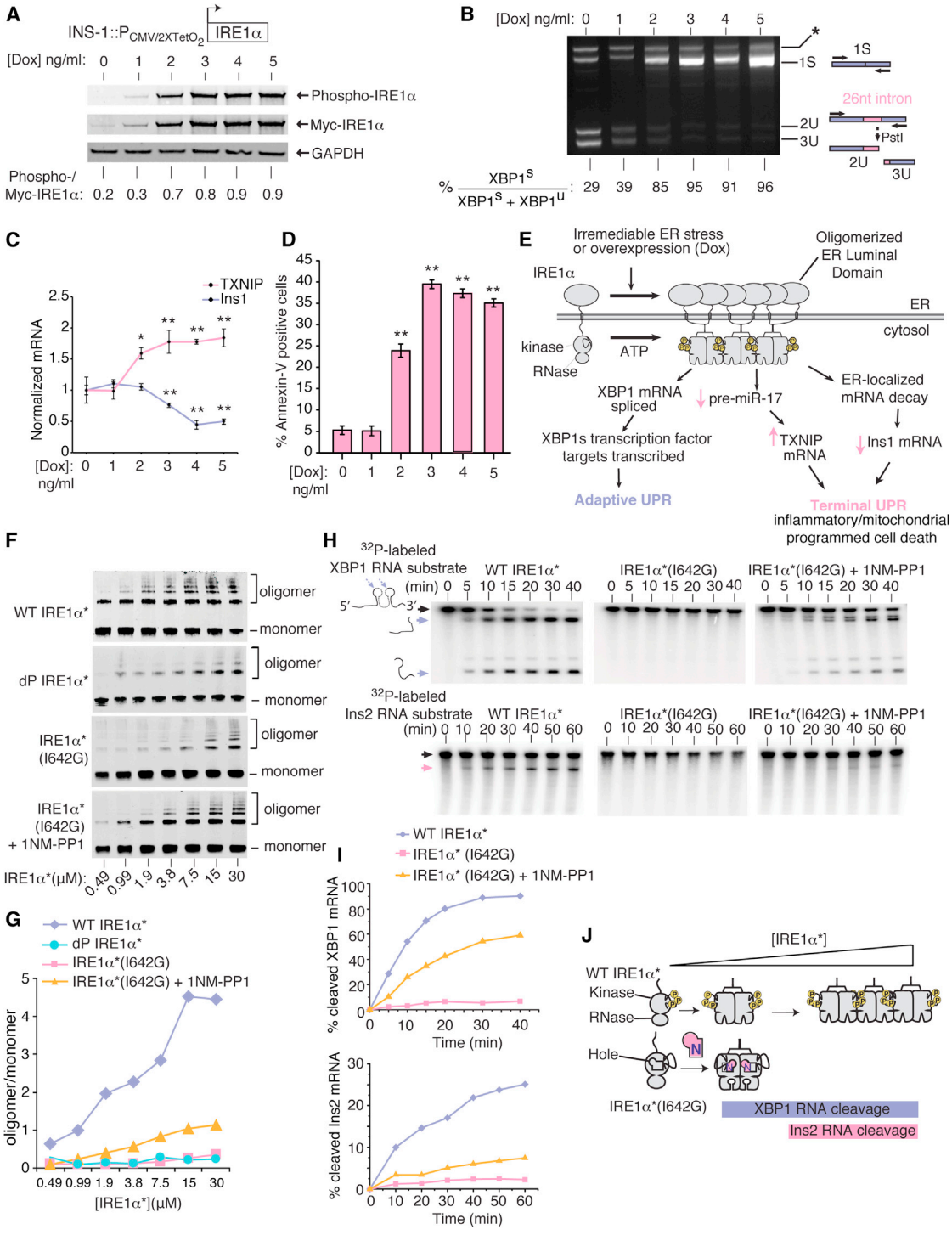


**Figure 1. IRE1α's Kinase Uses Homo-Oligomerization as a Rheostat to Control RNase Activity and Apoptosis**

(A) Anti-phospho-IRE1α and anti-Myc immunoblots (ratiometric quantitation, normalized to GAPDH).

(B) Agarose gel of PstI-digested XBP1 cDNA amplicons (ratiometric quantitation of spliced to total XBP1 cDNAs).

(C) qPCR for Insulin1 (Ins1) and TXNIP mRNAs.

(D) Percent of Annexin-V positive staining. (A)–(C) utilized INS-1::IRE1α (WT) cells under increasing [Dox] at 24 hr, whereas (D) is at 72 hr.

(E) Model of how IRE1α promotes both adaptive and apoptotic outputs.

(F and G) (F) Immunoblots of increasing concentrations of IRE1α*(WT), dP-IRE1α*(WT), and IRE1α*(I642G) −/+ 1NM-PP1 (10 μM) followed by disuccinimidyl suberate (DSS) (250 μM) crosslinking with oligomer/monomer quantification (G).

*(legend continued on next page)*

Consistent with partial increases in oligomeric state, RNase activity is revived in 1NM-PP1-bound IRE1α* (I642G) but with activity largely confined to XBP1 RNA (Figures 1H and 1I). Therefore, both IRE1α* and 1NM-PP1-bound IRE1α* (I642G) efficiently cleave XBP1 RNA, but only IRE1α* surpasses the oligomerization threshold needed to catalyze the more sluggish Ins2 RNA cleavage reaction (Figure 1J). Thus, oligomerization state directly impacts IRE1α's RNA substrate specificity.

We next tested effects in vivo. Upon self-association of its lumenal domains when expressed in an INS-1 line, IRE1α (I642G) fully splices XBP1 mRNA under 1NM-PP1 without ER stress and without causing Ins1 mRNA decay or apoptosis (Figure S1G). In fact, without 1NM-PP1, IRE1α (I642G) even reduces apoptosis under ER stress, acting as a strong dominant negative (Figure S1H). Another kinase-dead mutant, IRE1α (K599A) (which is also RNase dead), and an RNase-dead mutant, IRE1α (N906A), are also strongly dominant negative for apoptosis (Figure S1H).

We previously showed that, by pre-emptively producing XBP1s, 1NM-PP1-activated IRE1α (I642G) provides a metastable degree of cytoprotection against subsequent ER stress (Han et al., 2008, 2009), as does forced expression of XBP1s, shown here (Figure S1I). However, without a window of sufficient time to permit adaptive preconditioning, simultaneous provision of 1NM-PP1 and ER stress agents rescues Ins1 mRNA decay and apoptosis in a 1NM-PP1 dose-dependent manner (Figures S1J and S1K).

Further supporting the notion that IRE1α triggers apoptosis using its RNase, a "holed"-RNase-dead double mutant—IRE1α (I642G/N906A)—remains dominant negative under 1NM-PP1 (Figure S1L). In aggregate, the chemical-genetic studies show that the oligomeric state of IRE1α kinase/RNase subunits impacts both RNA substrate selection and cell fate and that discrete, intermediate activation states are available to the effector catalytic domains (Figure S1M).

## Divergent Allosteric Modulation of IRE1α Oligomeric State and RNase Activity with Distinct Kinase Inhibitors

As with the rationally engineered mutants, we find that intermediate activation states in IRE1α occur naturally through rare somatic *Ire1α* gene mutations found in human cancers, including glioblastoma, lung adenocarcinoma, and serous ovarian cancer (Greenman et al., 2007). We predicted that five mutations spanning the kinase and RNase should affect function: four are missense, and one, Q780Δ, which is nonsense, amputates the entire RNase (Figure 2A). Expressed conditionally in isogenic INS-1 lines, the human IRE1α cancer mutants are all compromised for apoptosis (Figure 2B). Normalized to WT, the mutations significantly abrogate autophosphorylation and XBP1 splicing (Figures 2C–2E). Expression of severely crippled IRE1α (Q780Δ) or IRE1α (P830L) actually increases Ins1 mRNA levels (Figure 2F), suggesting that some basal decay may even be blocked. Cells expressing IRE1α (Q780Δ) or IRE1α (P830L) proliferate well, in contrast to those expressing IRE1α (WT) or parental lines under ER stress (Figure 2H) (Movies S1, S2, S3, S4, S5, and S6). The mRNA encoding cyclin-dependent kinase inhibitor p21 is strongly induced in cells expressing IRE1α (WT), but not IRE1α (Q780Δ) or IRE1α (P830L) (Figure 2I). Marking cycling cells, Ki67 sharply declines upon expression of IRE1α (WT), but not IRE1α (Q780Δ) or IRE1α (P830L) (Figure 2J).

Lack of the RNase in IRE1α (Q780Δ) converts it into a dominant negative (Figures S2A–S2D). The P830L mutation, which occurs at the kinase/RNase junction (Figure 2G), may destabilize a dimerization interface (Xue et al., 2011). We predicted and tested that RNase activity in IRE1α (P830L) can be rescued with a kinase inhibitor, as IRE1α (I642G) can with 1NM-PP1.

We previously employed two distinct classes of kinase inhibitors—types I and II—to stabilize alternate kinase active site conformations in IRE1α (Wang et al., 2012). APY29 is a type I kinase inhibitor of IRE1α that stabilizes an active kinase domain conformation, which is typically adopted by ATP-bound kinases. By stabilizing the active kinase conformation, type I inhibitors act as ligands that allosterically activate IRE1α's RNase—e.g., 1NM-PP1 is a type I inhibitor of IRE1α (I642G).

Compared to IRE1α* (WT), IRE1α* (P830L) has reduced kinase activity (Figure 3A), as the full-length protein does in vivo (Figure 2C). APY29 dose-dependently suppresses residual autophosphorylation of IRE1α* (P830L) (Figure 3B). IRE1α* (P830L) cannot cleave a FRET-quenched XBP1 RNA minisubstrate (Han et al., 2009) (Figures 3C–3E), which is consistent with reduced RNase activity in vivo (Figure 2D). But, opposite to effects on kinase activity, APY29 increases IRE1α* (P830L)'s oligomeric state to rescue RNase activity (Figures 3D–3G).

If, as all preceding results suggest, kinase-driven oligomerization of IRE1α hyperactivates its RNase to trigger apoptosis, then kinase inhibitors that block oligomerization should prevent apoptosis under ER stress. To this end, we employed type II kinase inhibitors that stabilize an inactive ATP-binding site conformation in IRE1α. We previously developed a subset of type II kinase inhibitors designated KIRAs, for *k*inase-*i*nhibiting *R*Nase-*a*ttenuators, that inhibit IRE1α's RNase activity by breaking oligomers (Wang et al., 2012). Since our original report, we have identified KIRA6 as a more potent version (Figure 3H). KIRA6 dose-dependently inhibits IRE1α* (WT) kinase activity, XBP1 RNA cleavage, Ins2 RNA cleavage (with lower $IC_{50}$ than for XBP1 RNA in a competition assay), and oligomerization (Figures 3I–3L).

To follow IRE1α oligomerization in vivo, we first tested a reporter called IRE1-3F6HGFP that contains an EGFP domain positioned near the kinase (Li et al., 2010), but found that it has attenuated XBP1 splicing and fails to induce apoptosis (Figures S3A and S3B). To avoid potential steric effects on the kinase, we constructed a superfolder green fluorescent protein (sfGFP)

(H and I) (H) Time course urea PAGE of cleavage of $\alpha^{32}$P-labeled XBP1 RNA and Insulin2 (Ins2) RNA by IRE1α*(WT) and IRE1α*(I642G) −/+ 1NM-PP1 (10 μM), with quantification (I).

(J) Model of oligomerization dependence of RNase activity against XBP1 and Ins2 RNAs by IRE1α*(WT) and IRE1α*(I642G). Three independent biological samples were used for XBP1 splicing, qPCR, and Annexin V experiments. Data are plotted as mean value ± SD. *$p < 0.05$ and **$p < 0.01$, ns, not significant.

See also Figure S1.

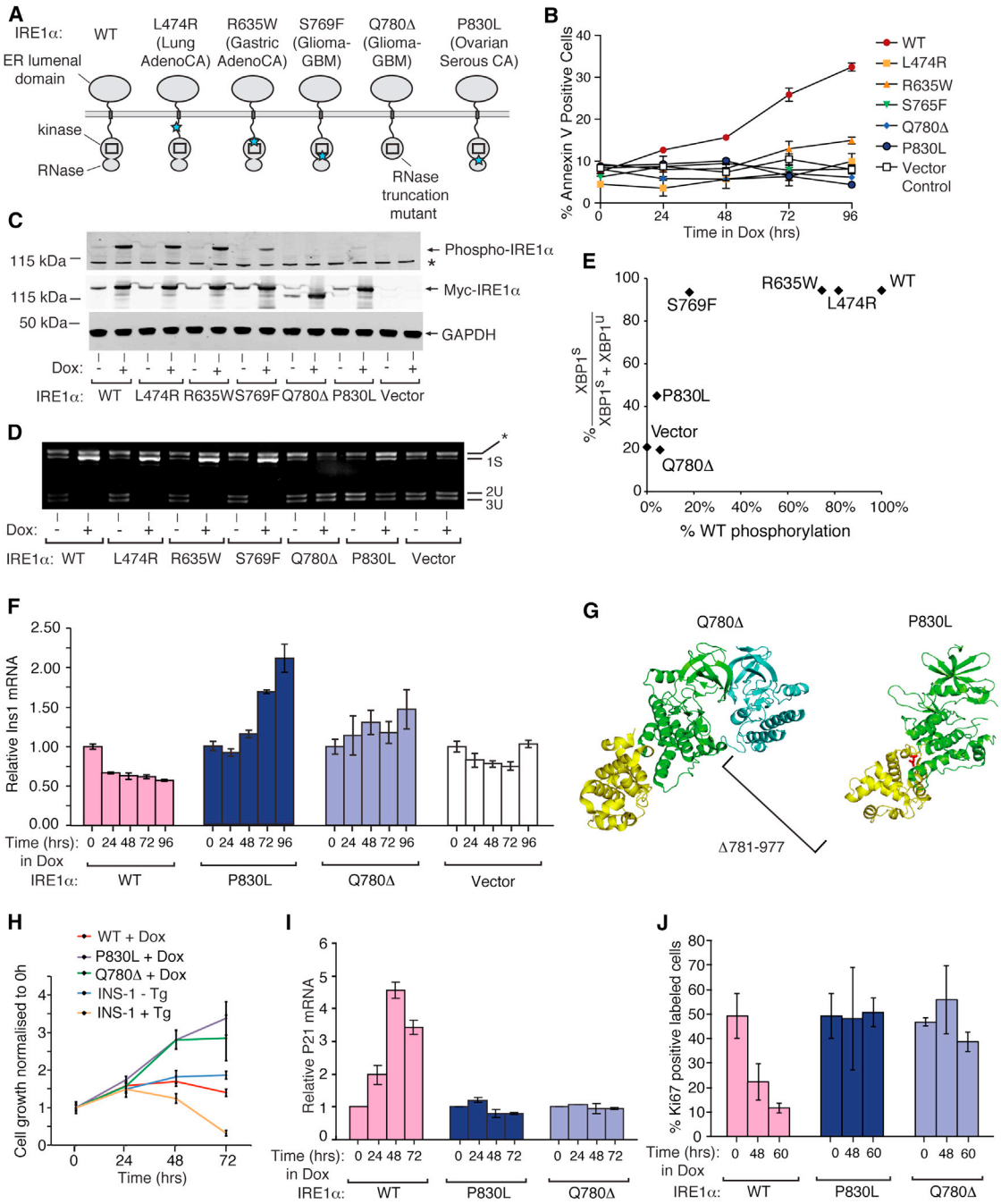


**Figure 2. IRE1α Cancer Mutants Are Disabled for Apoptosis**

(A) Cancer-associated mutations in human IRE1α.

(B) Time course Annexin-V staining of INS-1 cells stably expressing human IRE1α (WT), (L474R), (R635W), (S765F), (Q780*), and (P830L) under saturating Dox (1 μg/ml).

(C and D) (C) Anti-phospho-IRE1α and anti-Myc immunoblots and (D) agarose gel of PstI-digested XBP1 cDNA amplicons from INS-1 cells expressing human IRE1α (WT) and mutants with Dox (1 μg/ml) for 24 hr.

(E) XBP1 splicing from (D) as a function of IRE1α phosphorylation from (C).

(F) Time course qPCR of Ins1 mRNA from INS-1 cells expressing IRE1α (WT) and mutants under Dox (1 μg/ml).

(G) Cartoon of monomeric human IRE1α (P830L) (right) and IRE1α (Q780*) dimerized with a IRE1α (WT) subunit (left) based on PDB: 3P23.

(H) Time course MTT staining of INS-1 cells expressing IRE1α (WT), IRE1α (P830L), or IRE1α (Q780*) −/+ Dox (1 μg/ml) or parental INS-1 cells −/+ 100 nM Tg.

(I and J) Time course qPCR for p21 mRNA and Ki67 staining from INS-1 IRE1α (WT), IRE1α (P830L), or IRE1α (Q780*) cells under Dox (1 μg/ml). Three independent biological samples were used for qPCR, Ki67, and Annexin V experiments. Data are plotted as mean ± SD.

See also Figure S2.

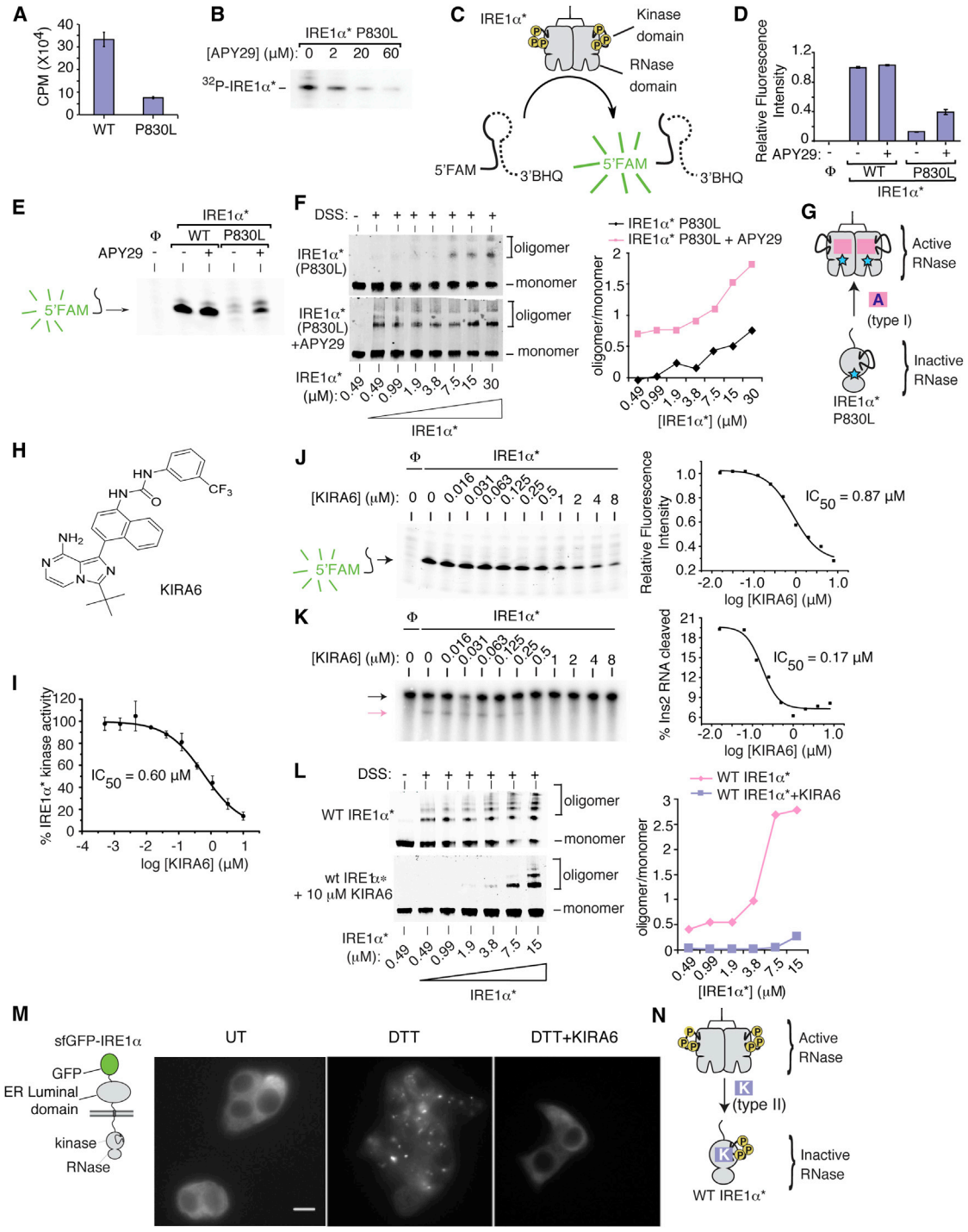


**Figure 3. Divergent Modulation of IRE1α RNase Activity Using Distinct Classes of Kinase Inhibitors**

(A) Phosphorimager analysis of human IRE1α* (25 nM) and IRE1α* (P830L) (25 nM) kinase activity against peptide substrate (PAKtide, 2 μM) in the presence of $^{32}$Pγ-ATP.

(B) Autoradiogram of IRE1α* (P830L) autophosphorylation under increasing [APY29].

(C) 5′ FAM-3′ BHQ XBP1 minisubstrate to measure RNase activity.

(D) RNase activities of IRE1α* and IRE1α* (P830L) −/+ APY29 (20 μM) per (C).

(E) Urea PAGE of XBP1 cleavage products from (D).

(F) Immunoblots of increasing IRE1α* (P830L) after incubation with DMSO or APY29 (200 μM) and DSS with oligomer/monomer quantification.

(G) Model of APY29 rescue of oligomerization and RNase activity in IRE1α* (P830L).

*(legend continued on next page)*

N-terminally fused to the ER lumenal domain. Expressed isogenically in INS-1 cells, sfGFP-IRE1α retains apoptotic activity and gathers into discrete fluorescent foci in the ER membrane under the ER stress agent dithiothreitol (DTT) (Figures 3M, S3A, and S3B). A (I642G) version of sfGFP-IRE1α fully splices XBP1 mRNA under 1NM-PP1 without forming foci (Figures S3C and S3D). In fact, without 1NM-PP1, sfGFP-IRE1α (I642G) resists forming foci under DTT, suggesting that, without its ligand, it adopts an inactive kinase conformation and explains dominant-negative effects of IRE1α (I642G) (Figure S1H). Similar to apoptosis, foci formation by sfGFP-IRE1α (I642G) requires both ER stress and 1NM-PP1, further supporting the tight link between IRE1α oligomerization—shown in vivo through foci—and apoptosis. Thus, using sfGFP-IRE1α, which faithfully recapitulates cytosolic events, we tested and found that KIRA6 prevents foci formation by DTT (Figure 3M). Hence, KIRAs fulfill their design principle of breaking kinase/RNase oligomers to inhibit the RNase (Figure 3N).

### KIRA6 Inhibits IRE1α In Vivo to Preserve Cell Viability and Function in Diverse Cells and Rodent Tissues Experiencing ER Stress

The remainder of our work focused on testing physiological effects of IRE1α kinase inhibition. APY29 showed pleiotropic toxicity, including proliferative blocks at low micromolar concentrations, precluding further in vivo testing of ON-target effects (Figure S4A). In contrast, KIRA6 had negligible toxicity up to 10 μM (Figure S4A), providing a favorable therapeutic index to test cytoprotection. INS-1 lines confirmed ON-target effects: pro-Caspase-3 cleavage upon IRE1α (WT) expression is prevented by KIRA6 (Figure 4A). Moreover, despite its inability to directly inhibit JNK activity in vitro, KIRA6 strongly inhibits JNK phosphorylation from IRE1α hyperactivation or ER stress (Figures 4A–4C). Also, KIRA6 dose-dependently inhibits Ins1 mRNA decay, proinsulin depletion, and apoptosis from IRE1α hyperactivation (Figures 4D–4F).

Chemical-genetic tools enabled ON-target competition tests. KIRA6 (1) reduces 1NM-PP1-induced XBP1 RNA cleavage by IRE1α* (I642G) in vitro (Figure 4G); (2) antagonizes 1NM-PP1-induced XBP1 splicing by IRE1α (I642G) in vivo (Figure 4H); and (3) reduces 1NM-PP1 potentiation of Ins1 mRNA decay and apoptosis during ER stress in a dose-dependent manner (Figures 4I, S4B, and S4C). KIRA6 does not inhibit the activity of a panel of Ser/Thr kinases (including JNK2 and 3) in vitro (Figure S4D). Moreover, KIRA6 does not inhibit or secondarily promote eIF2α phosphorylation by PERK, the other UPR kinase (Figure S4E).

Having confirmed that KIRA6 has ON-target effects, we next tested efficacy against endogenous IRE1α using the established ER stress regimes in their linear ranges straddling the apoptotic trigger point (Figures S1A–S1D). In INS-1 cells, KIRA6 inhibits IRE1α autophosphorylation by Tg and XBP1 mRNA splicing by Tm in a dose-dependent manner (Figures 5A–5C), whereas a control analog, (NMe)KIRA6, incapable of binding to the kinase hinge region inhibits neither output at 10 μM (Figures 5A, 5B, S5A, and S5B).

We next tested multiple terminal UPR endpoints and found that KIRA6: (1) inhibits Ins1 and Ins2 mRNA decay by Tm in INS-1 cells in a dose-dependent manner (Figures 5D and S5C). We noted that the in vivo $IC_{50}$ of KIRA6 for Ins1 mRNA rescue is lower than that for inhibiting XBP1 splicing, and Ins2 mRNA levels recover even at 20 nM KIRA6 and exceed basal, untreated levels in a dose-dependent manner. Furthermore, KIRA6 (2) inhibits TXNIP induction by Tm in murine C57BL/6 pancreatic islets (Figure 5E); (3) inhibits IRE1α-dependent activation of a TXNIP 3′ UTR luciferase reporter containing its two miR-17 binding sites (Figure S5D); (4) prevents 1L-1β secretion by Tm and Tg (but not ATP) in THP1 macrophage lines (Figure 5F); (5) prevents loss of INS-1 Ki67-positive cells and C57BL/6 pancreatic islet double-positive Nkx6.1/EdU β cells under ER stress (Figures 5G, 5H, and S5E) (Movie S7); (6) dose-dependently inhibits apoptosis of INS-1 cells under BFA (Figure 5I); (7) reduces TUNEL staining of β cells in C57BL/6 and human islets under Tm (Figures 5J and S5F); and (8) preserves glucose-stimulated insulin secretion (GSIS) in C57BL/6 islets under Tm (Figure 5K).

We also tested effects of STF-083010, a small-molecule tool compound that reactively modifies Lysine 907 in the RNase active site (Papandreou et al., 2011) (Figure S5G). As with KIRA6, STF-083010 (at 50 μM) also decreases Ins1 mRNA decay under IRE1α hyperactivation and apoptosis by Tm (Figures S5H and S5I). Moreover, when used in combination at doses that are subtherapeutic individually, STF-083010 (1 μM) and KIRA6 (50 nM) afford significant cytoprotection under Tm (Figure S5J). Together, these data further implicate IRE1α's RNase in promoting apoptosis, in this case by showing that the RNase can even be inhibited combinatorially through two distinct sites in IRE1α for cytoprotection.

To rule out the possibility that KIRA6 defeats ER stress agents upstream of IRE1α, we tested whether blocks to ER posttranslational modification still persist under KIRA6. A test substrate, the null Hong Kong variant of alpha-1 anti-trypsin (NHK-A1AT), normally glycosylated and ER-retained, is deglycoslyated under Tm. NHK-A1AT clearly remains deglycoslyated under both Tm and KIRA6 (Figure 5L).

Encouraged by clear and convincing evidence that KIRA6 preserves cell viability and function in multiple cell and explant systems under diverse ER stress regimes, we next applied a higher evidentiary standard by testing disease-relevant animal models.

(H) Structure of KIRA6.
(I) KIRA6 inhibition of IRE1α* kinase activity. $IC_{50}$ values by fitting percent kinase activity per assay in (A) (n = 3).
(J and K) (K) Urea PAGE of competition cleavage by IRE1α* of XBP1 RNA minisubstrate (J) and $\alpha^{32}$P-labeled Ins2 RNA (K) under indicated [KIRA6]; $IC_{50}$s by fitting in-gel fluorescence intensities (XBP1) and phosphorimager (Ins2).
(L) Immunoblots of increasing [IRE1α*] incubated with DMSO or KIRA6 (10 μM) and DSS with oligomer/monomer quantification.
(M) Left, cartoon of sfGFP-IRE1α reporter. Right, images of sfGFP-IRE1α induced with (subapoptotic) 1 ng/ml Dox for 24 hr in INS-1 cells −/+ DTT (5 mM) for 1 hr −/+ KIRA6 (1 μM). Scale bar, 5 μm.
(N) Model for how KIRA6 lowers oligomeric status and RNase activity of IRE1α*. Data are plotted as mean ± SD.
Also see Figure S3.

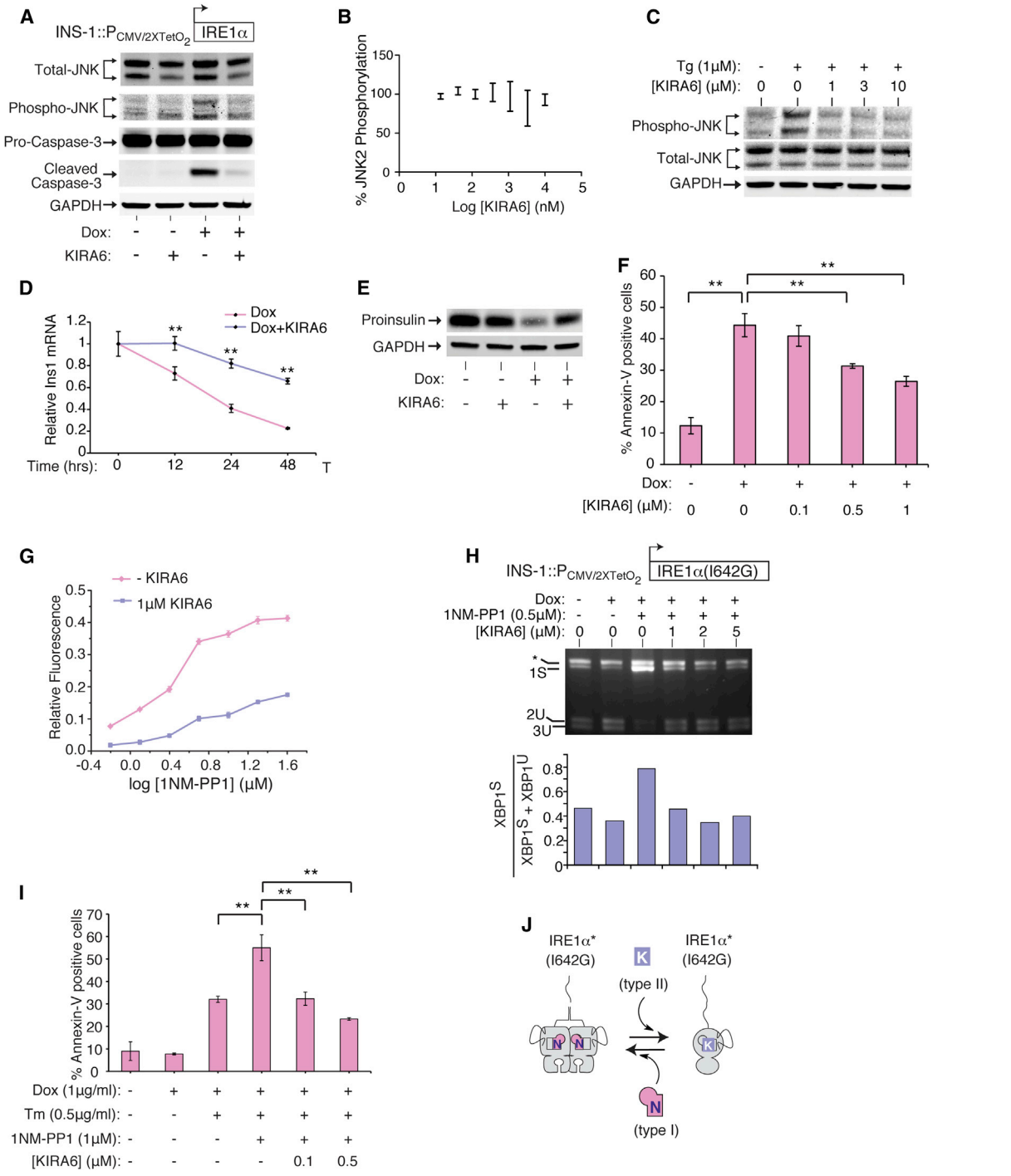


**Figure 4. KIRA6 Inhibits IRE1α Terminal UPR Outputs and Apoptosis**

(A) Anti-total JNK, anti-phospho-JNK, and anti-Pro- and cleaved Caspase-3 immunoblots of INS-1 IRE1α (WT) cells treated with Dox (5 ng/ml) −/+ 1 μM KIRA6 for 72 hr.

(B) JNK2α1 phosphorylation under indicated [KIRA6] by in vitro ELISA-based anti-phospho-JNK assay.

(C) Anti-total and phospho-JNK immunoblots of INS-1 cells pretreated for 1 hr with indicated [KIRA6] and then 1 μM Tg for 2 hr.

(D) qPCR for Ins1 mRNA in INS-1 IRE1α (WT) cells treated with Dox (5 ng/ml) −/+ KIRA6 (1 μM).

(E) Anti-proinsulin immunoblot of samples in (A).

(F) Percentage of Annexin V staining in INS-1 IRE1α (WT) cells after 72 hr in Dox (5 ng/ml) and indicated [KIRA6].

(G) Competition between indicated [1NM-PP1] and KIRA6 (1 μM) for IRE1α* (I642G) RNase.

*(legend continued on next page)*

Given compelling evidence that ER stress contributes to photoreceptor loss in many retinal diseases, including retinitis pigmentosa (RP) (Zhang et al., 2014), we tested KIRA6 in two rodent models. Transgenic rats expressing a misfolded Rhodopsin mutant (P23H) exhibit spontaneous photoreceptor degeneration and are a model of autosomal dominant RP (Gorbatyuk et al., 2010). Retinas of hemizygous P23H rats develop normally but lose photoreceptors beginning on postnatal day (P) 10; by P40, the outer nuclear layer (ONL), representing photoreceptor nuclei, is reduced to ~50% of the thickness of WT rats (Pennesi et al., 2008). We intravitreally injected KIRA6 or carrier into either eye of individual P23H rats at P9 and P15. ONL thickness at P40 revealed partial yet statistically significant protection from photoreceptor loss in KIRA6-treated eyes (Figures S6A and S6B).

Given rapid clearance of intravitreally injected small molecules (half-life < 60 hr), we were unable to maintain sufficient KIRA6 in the vitreous over the ~30 day progression of retinal degeneration in P23H rats to test for functional protection. Therefore, we used a model of acute photoreceptor loss occurring over 7 days from a single intravitreal injection of Tm into adult rats (Shimazawa et al., 2007). Intravitreal coinjection of KIRA6 with Tm significantly reduces XBP1 splicing, TXNIP induction, and decay of the ER-localized photoreceptor-specific Rhodopsin mRNA (Figures 6A–6C). Rhodopsin mRNA may be an IRE1α RNase substrate because Rhodopsin RNA is cleaved by IRE1α*, but not RNase-dead IRE1α* (N906A), at a G/C site with flanking similarity to scission sites in XBP1 (Figure S6C). KIRA6 dose-dependently inhibits Rhodopsin RNA cleavage by IRE1α* (Figures 6F and 6G). Concomitant with blockage of terminal UPR outputs, coinjection of KIRA6 in the Tm model reduces photoreceptor loss by optical coherence tomography (OCT) and histology (Figure 6H).

Next, to test whether KIRA6 also provides functional protection, we established a dose-response curve to determine threshold [Tm] that causes functional retinal damage as measured by scotopic electroretinograms (ERG) (Figure 6I). Based on the results, we injected Tm at 3 μg/ml. In this regime, coinjection with KIRA6 substantially protects against loss of ERG responsiveness, significantly preserving both a and b wave amplitudes (Figures 6J, 6K, and S6D).

Finally, to test in vivo efficacy of systemic KIRA6, we chose the *Ins2*$^{+/Akita}$ (Akita) mouse, which expresses a mutant (C96Y) proinsulin unable to complete oxidative folding, thus causing chronic ER stress, β cell apoptosis, and diabetes in infancy (Lerner et al., 2012). The pharmacokinetic profile of KIRA6 in BALB/c mice intraperitoneally (i.p.) dosed at 10 mg/kg showed good drug plasma AUC levels (AUC 0–24 hr = 14.3 μM*h) with moderate clearance (22.4 ml/min/kg). Drug half-life was 3.90 hr, $C_{max}$ was 3.3 μM, and plasma levels at 4 and 8 hr were 1.2 μM and 0.33 μM, respectively. Initial systemic studies utilized a Tm i.p. challenge in C57BL/6 mice, with and without KIRA6 coinjection, and UPR markers measured in liver. Low-dose Tm (2 μg/kg) elevates liver XBP1 splicing without decay of ER-localized Blos1 mRNA (Hollien et al., 2009), whereas KIRA6 coprovision reduces XBP1 splicing (Figures S7A and S7B). Escalation of Tm to 100 μg/kg further increases XBP1 splicing and triggers Blos1 mRNA decay, with both markers attenuated by KIRA6 (Figures S7C and S7D).

Based on low micromolar KIRA6 needed for protection in cell culture, we chose i.p. dosing regimens of 5 or 10 mg/kg twice a day (b.i.d.) for Akita chronic efficacy studies to provide similar exposure. We injected KIRA6 into randomized 3-week-old male Akita mice when their random blood glucose levels were at prediabetic range (~200 mg/dl). In both dosing regimes, we observed significant amelioration of random glucose levels over several weeks in KIRA6-treated mice compared to vehicle, both fed ad lib (Figures 7A and S7E). TXNIP mRNA levels decline in islets of KIRA6-treated mice within 1 week without compensatory increase of CHOP mRNA (downstream of PERK) (Figures S7G and S7H). KIRA6-treated mice appeared healthy even after 49 days from initial injection and displayed no significant differences in weight from vehicles (Figures 7B and S7F). Even 12 days after stopping injections, the 5 mg/kg KIRA6-treated mice show significantly improved random blood glucose levels and glucose tolerance tests (GTT) (Figure 7C). Even 21 days after stopping injections, KIRA6-treated mice display statistically significant doubling in both plasma insulin and C-peptide levels (Figures 7D and 7E). Hematoxylin and eosin staining (H&E) and insulin staining of whole pancreas sections revealed increased islet size in KIRA6-treated animals (Figures 7F and 7G). Insulin-positive islet areas remained significantly higher in the KIRA6-treated group 18 days after stopping injections (Figure 7H).

## DISCUSSION

In the baker's yeast *S. cerevisiae*, the UPR is a homeostatic signaling pathway controlled by IRE1-mediated splicing of an mRNA encoding an adaptive transcription factor called Hac1 (Cox and Walter, 1996). Following this paradigm from this unicellular eukaryote, reports have suggested that the signaling outputs of mammalian IRE1α are likewise solely restricted to restoring homeostasis and promoting survival under ER stress (Lin et al., 2007). Furthermore, these models posit that, when ER stress becomes irremediable, IRE1α's prosurvival signaling through XBP1 splicing circumstantially wanes (through an unknown mechanism), even as apoptotic outputs from PERK rise to promote cell death, without further opposition by IRE1α (Lin et al., 2009). These arguments therefore predict that sustained IRE1α activation (even if artificially imposed) should universally promote cell survival under ER stress, whereas genetic or pharmacological inhibition of IRE1α should hasten cell death. Through forcibly activating and inhibiting IRE1α in a variety of cell systems and animal models, here we generated extensive

(H) Agarose gel of PstI-digested XBP1 cDNA amplicons from INS-1 cells IRE1α (I642G) cells induced by Dox (1 μg/ml) for 24 hr, then 1NM-PP1 (0.5 μM) −/+ indicated [KIRA6] for 3 hr with quantitation.

(I) Annexin V staining of INS-1 IRE1α (I642G) cells after 72 hr with Dox (1 μg/ml), Tm (0.5 μg/ml), 1NM-PP1 (1 μM), and indicated [KIRA6].

(J) Model of 1NM-PP1 and KIRA6 competition of oligomerization and RNase activity in IRE1α* (I642G). Data are plotted as mean ± SD. *p < 0.05 and **p < 0.01. See also Figure S4.

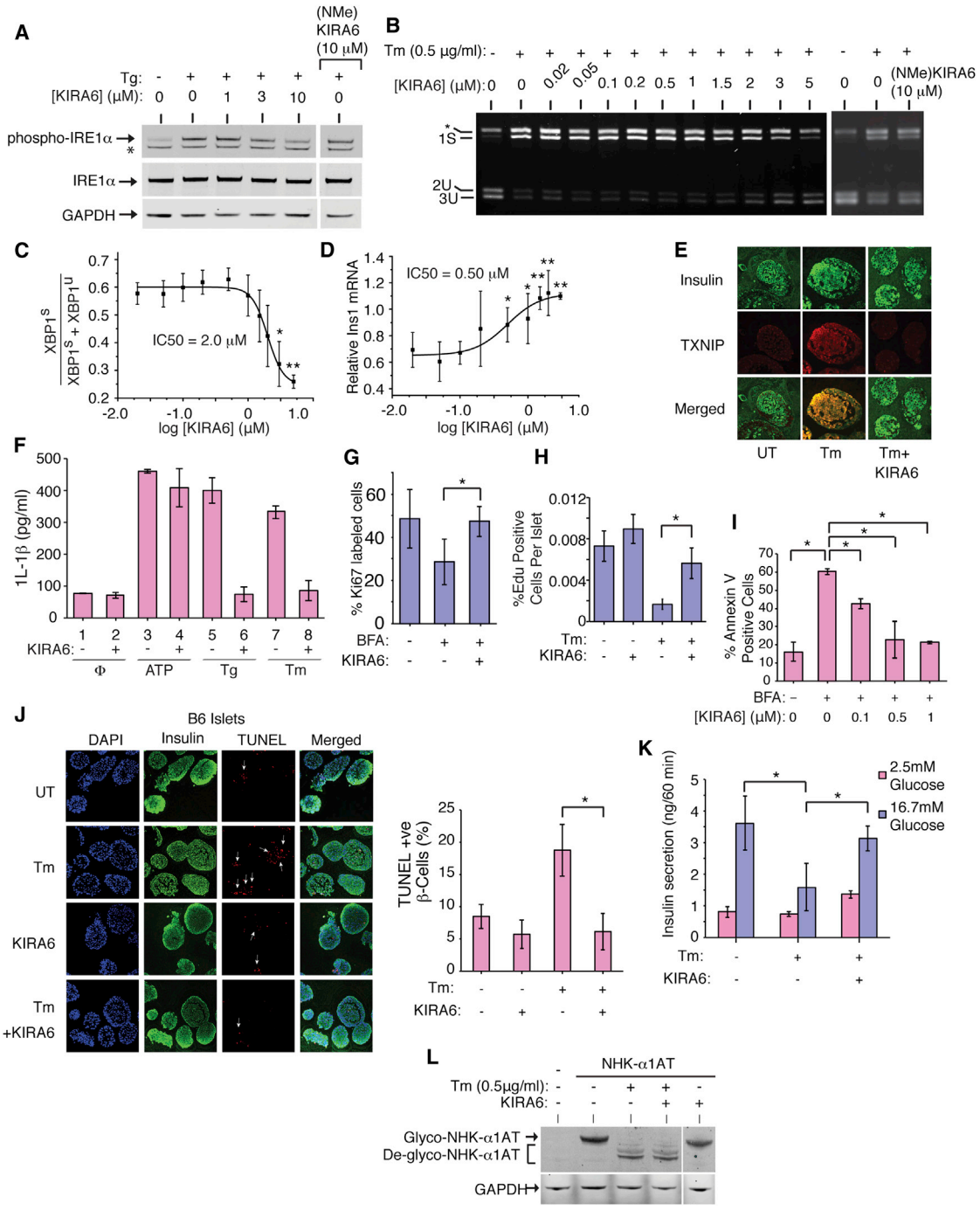


**Figure 5. KIRA6 Reduces ER Stress-Induced Death of Cultured Cells and in Pancreatic Islet Explants**

(A) Immunoblots for total and phospho-IRE1α in INS-1 cells pretreated for 1 hr with indicated [KIRA6] or 10 μM (NMe)KIRA6 and then Tg (1 μM) for 2 hr.

(B) Agarose gel of XBP1 cDNA amplicons from INS-1 cells pretreated with indicated [KIRA6] for 1 hr or 10 μM (NMe)KIRA6, followed by 0.5 μg/ml Tm for 8 hr.

(C) Ratios of $XBP1^S$ over ($XBP1^S$ + $XBP1^U$) from (B).

(D) qPCR for Ins1 mRNA (normalized to no Tm) in INS-1 cells pretreated for 1 hr with indicated [KIRA6] and then 12 hr in Tm (0.5 μg/ml).

(E) Immunofluorescence: insulin (green) and TXNIP (red) in islets of C57BL/6 mice under 0.5 μg/ml Tm −/+ 0.5 μM KIRA6 for 16 hr.

(F) IL-1β secretion from THP-1 cells after 4 hr −/+ 0.5 μM KIRA6, 5 μg/ml Tm, 1 μM Tg, or 5 mM ATP.

(G) Ki67+ INS1 cells under 0.25 μg/ml BFA −/+ 0.5 μM KIRA6 for 48 hr.

(H) Proliferating mouse islet β cells under 0.5 μg/ml Tm −/+ 0.5 μM KIRA6 for 48 hr (nuclei double-positive for EdU and β cell nuclear marker, Nkx6.1, over total Nkx6.1 positive nuclei).

(I) Annexin-V staining of INS-1 cells treated with 0.25 μg/ml BFA and indicated [KIRA6] for 72 hr.

*(legend continued on next page)*

data that refute these aforementioned predictions to instead support opposite conclusions.

An alternative model that we previously proposed (Han et al., 2009) and mechanistically substantiated here is that IRE1α switches outputs depending on the level of ER stress. Under low, manageable levels of ER stress, adaptive UPR signaling promotes secretory homeostasis, partly through IRE1α-mediated splicing of XBP1 mRNA and consequent XBP1s outputs. Likewise, pre-emptive PERK activation affords a measure of cytoprotection against subsequent ER stress by attenuating translation (Lu et al., 2004), as does preconditioning with 1NM-PP1-bound IRE1α (I642G) to transiently stabilize an intermediate activation mode of the RNase confined to XBP1 splicing (Han et al., 2008).

However, under high ER stress, IRE1α acquires endonucleolytic activity against a large plethora of RNA targets, first identified in *D. melanogaster* and termed RIDD (Hollien and Weissman, 2006), including ER-localized mRNAs and noncoding RNAs in mammals (Han et al., 2009; Hollien et al., 2009; Lerner et al., 2012; Upton et al., 2012). These extra-XBP1 RNA cleavage events precede and closely track with entry of ER-stressed cells into apoptosis, and we showed here that their amelioration with small-molecule inhibitors of IRE1α kinase/RNase inhibits apoptosis. Thus, rather than have the two UPR kinases working in opposition, multiple lines of evidence suggest that a continuum of graded activation states (dependent upon the strength of upstream stress) is available to either IRE1α or PERK, both of which under high activation undergo switch-like conversion from promoting homeostasis to promoting cell death (Han et al., 2009; Lin et al., 2009). Similar switching mechanisms occur in other cell-surface death receptors that respond divergently depending on the strength or context of upstream inputs (Festjens et al., 2007; Ofengeim and Yuan, 2013).

Further supporting a model of binary, rather than unitary outputs, three postulates that we posed and tested reasonably establish causality between IRE1α hyperactivation and cell death:

(1) First, forced hyperactivation of IRE1α's RNase should suffice to lead cells into the terminal UPR and along a continuum of destructive outcomes, including proliferative blocks, loss of differentiated cell identity, and eventually into apoptosis. In line with this expectation, past a critical oligomerization threshold, IRE1α's RNase degrades key mediators of specialized cell function, including abundant insulin-encoding mRNAs in pancreatic β cells and rhodopsin mRNAs in retinal photoreceptor cells (both ER localized). Also, as previously shown, mRNAs encoding ER-resident enzymatic activities are also targeted by hyperactive IRE1α RNase, potentially compromising ER function (Han et al., 2009). Thus, at high activation, IRE1α's adaptive outputs become overshadowed by its destructive outputs and further amplified downstream by TXNIP, causing IL-1β secretion, sterile inflammation/pyroptosis (linked to both types 1 and 2 diabetes) (Lerner et al., 2012; Schroder et al., 2010), and JNK signaling (Urano et al., 2000). Further linking IRE1α to cell death, IRE1α cancer mutants show defective homo-oligomerization and RNase activity, which may allow the terminal UPR to become disabled or co-opted for survival advantage. Indeed, proliferative blocks normally imposed through IRE1α are defeated in the cancer mutants. Given these results, future studies of mutated IRE1α in cancer are warranted.

(2) Second, a class of IRE1α inhibitors that disrupt oligomerization should reduce RNase activity and terminal UPR events in tandem. Unique among multidomain kinases, the mechanistic relationship between IRE1α's kinase and RNase allows divergent small-molecule allosteric control (Wang et al., 2012). Whereas both are ATP competitive, IRE1α type I kinase inhibitors increase oligomerization to increase RNase activity, whereas IRE1α type II kinase inhibitors decrease oligomerization to decrease RNase activity. Here, we developed and tested the effects of KIRA6, an advanced IRE1α type II kinase inhibitor. Given that KIRA6 has a favorable therapeutic index and shows IRE1α ON-target effects, we predicted that it would reduce cell death under ER stress. Remarkably, blocking IRE1α with KIRA6 raises the apoptotic threshold and enhances survival during ongoing upstream ER stress, indicating that destructive signaling rather than a compromised ER microenvironment per se promotes cell death (Figure 7I). Although poly-pharmacological toxicity precluded testing ON-target effects of APY29, our results justify development and testing of nontoxic type I kinase inhibitors against IRE1α cancer mutants.

(3) Third, blocking IRE1α with KIRA6 should protect against ER stress-mediated cell degeneration in vivo, leading not only to increased cell survival but also to preserved physiological function. Consistent with this, in various cell types and explants, KIRA6 not only reduced cell loss under acute ER stress but also prevented proliferative blocks and preserved function (e.g., GSIS). Encouraged by these data, we tested KIRA6 in rodent models of chronic ER stress-induced retinal degeneration. P23H rats intravitreally treated with KIRA6 had significantly preserved photoreceptor numbers, and in the Tm coinjection model, functional protection was found. Finally, systemic administration of KIRA6 in the Akita diabetic mouse significantly reduced random blood glucose levels, improved glucose tolerance acutely, preserved β cells, and elevated blood insulin and C-peptide levels. Remarkably, beneficial effects persisted even several weeks after stopping treatment. To our knowledge, this is the first work showing small-molecule efficacy in the highly penetrant Akita genetic model.

(J) Immunofluorescence images of C57BL/6 islets treated with 0.5 μg/ml Tm −/+ 0.5 μM KIRA6 for 16 hr. Costained for DAPI (blue), insulin (green), and TUNEL (red). Quantification of TUNEL+ β cells (white arrows) normalized to DAPI+ cells.
(K) Glucose-stimulated insulin secretion (GSIS) by C57BL/6 islets after 0.5 μg/ml Tm −/+ 0.5 μM KIRA6 for 16 hr; [Glucose] was 2.5 mM or 16.7 mM for 60 min.
(L) Immunoblots for alpha-1 antitrypsin in HEK293 cells transfected with pCDNA3.1-α1hAT-NHK and then treated with KIRA6 (1 μM) −/+ Tm (0.5 μg/ml) for 20 hr.
Three independent biological samples were used for XBP1 splicing, qPCR, Annexin V, and immunofluorescence experiments. Data are plotted as mean ± SD. *$p < 0.05$ and **$p < 0.01$.
See also Figure S5.

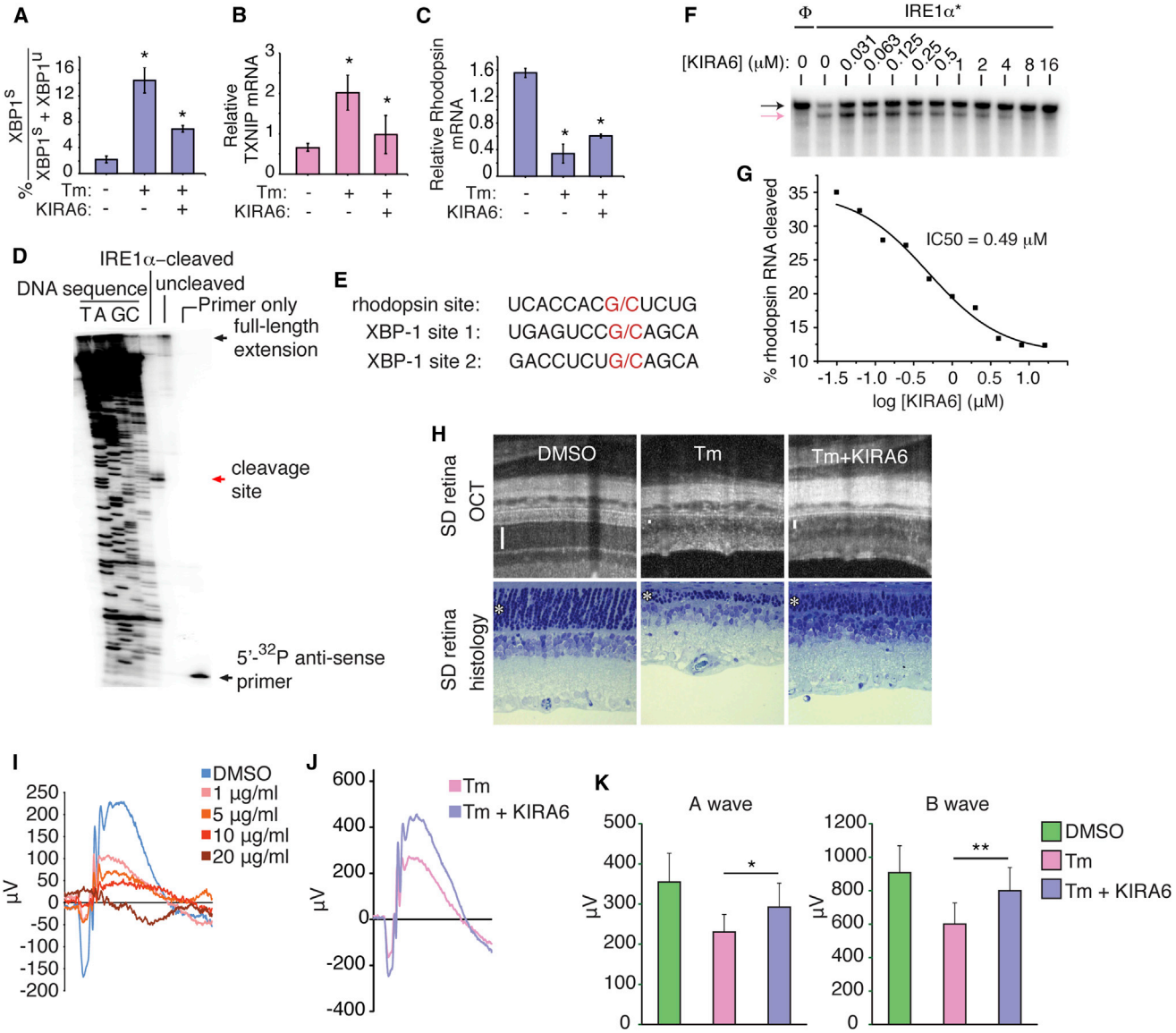


**Figure 6. Intravitreal KIRA6 Preserves Photoreceptor Cell Numbers and Function under ER Stress**

(A–C) (A) Percentage of XBP1 splicing in SD rat retinas 72 hr postintravitreal—and qPCR for TXNIP mRNA (B) and rhodopsin mRNA (C) 96 hr postintravitreal—injection of 20 μg/ml Tm −/+ 10 μM KIRA6.

(D–G) (D) Primer extension mapping of IRE1α cleavage site in rhodopsin RNA with alignment of rhodopsin and XBP1 mRNA (E). Urea PAGE of cleavage of $^{32}$P-labeled rhodopsin mRNA by IRE1α* with indicated [KIRA6], with $IC_{50}$ (G); black arrow: intact RNA; red arrow: cleaved RNA.

(H) OCT images and histological sections of SD rats 7 days postintravitreal injection of 20 μg/ml Tm −/+ 10 μM KIRA6; bars and asterisks denote ONLs.

(I) SD rats intravitreally injected at P21with 2 μl Tm or DMSO to achieve indicated [Tm]; ERG measurements at a light intensity of 0 dB recorded at P28.

(J) Representative scotopic ERG at a light intensity of 0 dB from a SD rat treated with Tm (3 μg/ml) ± KIRA6 (10 μM) at P21 and analyzed at P28.

(K) Quantified a and b wave amplitudes of 0 dB scotopic ERGs from SD rats treated with DMSO or Tm (3 μg/ml) ± KIRA6 (10 μM) at P21 and analyzed at P28. See also Figure S6.

Thus, we conclude that IRE1α exerts powerful effects on cell fate and function under ER stress and that its kinase domain presents an attractive target for small-molecule modulation. In summary, KIRA6, an advanced small-molecule kinase inhibitor of IRE1α, reduces cell death in several disease-relevant models of ER stress-induced cell degeneration. While homozygous deletion of either *Ire1α* or *Xbp1* impedes embryogenesis and secretory cell development (Reimold et al., 2001; Tirasophon et al., 1998; Urano et al., 2000; Zhang et al., 2005), the ability to titrate down IRE1α's catalytic activities with a small molecule provides an opportunity to uncouple extra-XBP1 destructive outputs from XBP1-dependent adaptation. From this work, we propose the existence of a natural therapeutic window for IRE1α inhibition owing to the higher oligomeric state

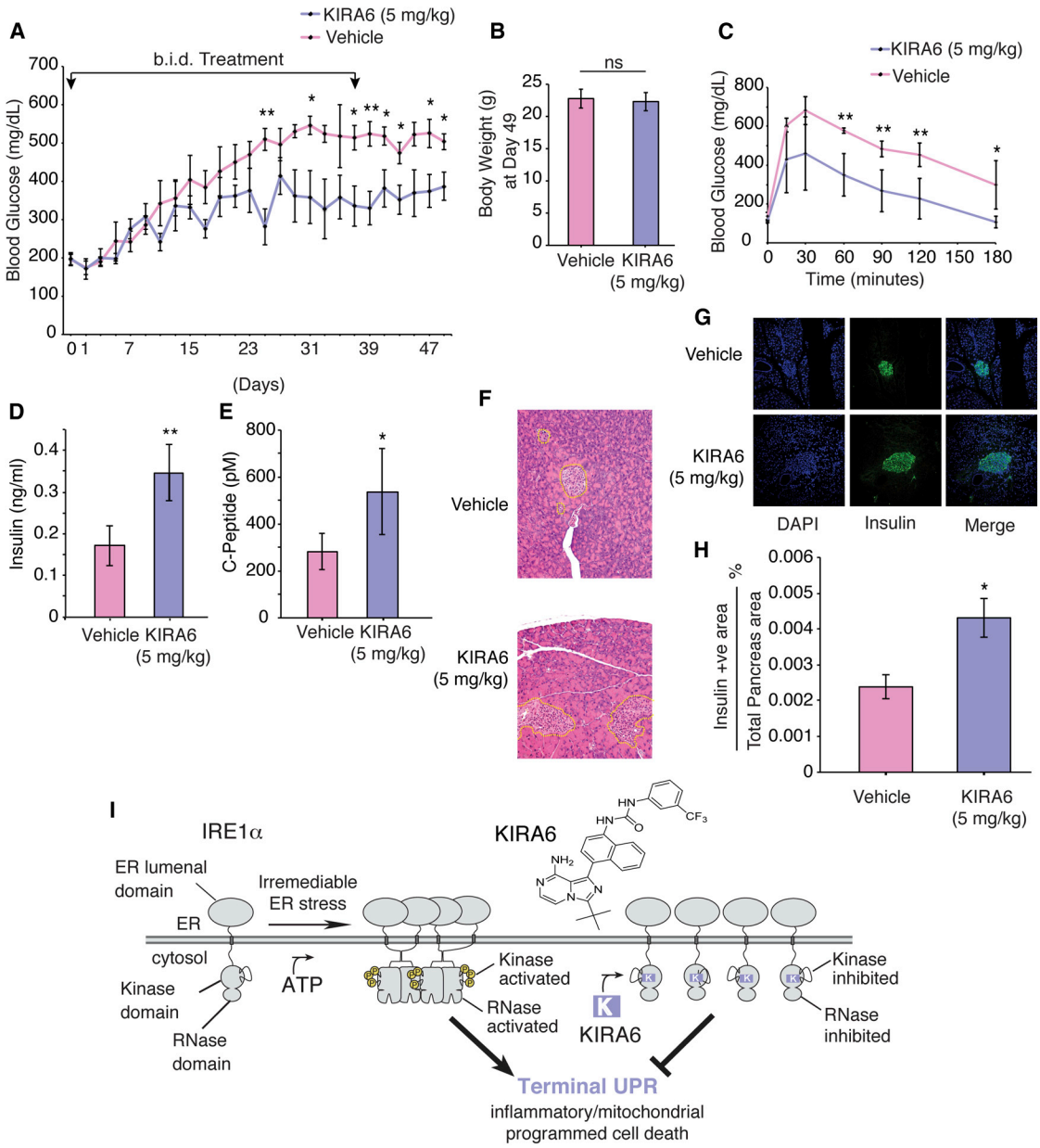


**Figure 7. Systemic KIRA6 Attenuates β Cell Functional Loss, Increases Insulin Levels, and Ameliorates Hyperglycemia in the Akita Mouse**

(A) Random AM blood glucose (BG) levels in male *Ins2*$^{+/Akita}$ mice i.p. injected for 37 days b.i.d. with KIRA6 (5 mg/kg) (n = 6) or vehicle (n = 6) starting at P21 (i.e., day 1). BGs (mean ± SEM), also analyzed by two-way RM ANOVA; p = 0.0122.

(B) Cohort body weights at day 49.

(C) Glucose tolerance tests on day 49 (12 day postinjections) of O/N fasted *Ins2*$^{+/Akita}$ mice (P53) after i.p. (2 g/kg) glucose (KIRA6 n = 6, vehicle n = 3).

(D and E) Random insulin and C-peptide levels in *Ins2*$^{+/Akita}$ mice on day 58 (21 days postinjections). KIRA6 (5 mg/kg) (n = 5) and vehicle (n = 4).

(F) Whole pancreatic histological sections from *Ins2*$^{+/Akita}$ mice on day 53 (15 days postinjections). Islets delineated by dashed outline.

(G) Immunofluorescence micrographs of samples in (F): costained for DAPI (blue) and insulin (green) with merge.

(H) Total β cell area as a percentage of total pancreas area on day 55 (18 day postinjections). KIRA6 (5 mg/kg) (n = 6) and vehicle (n = 3).

(I) Model of how KIRA6 prevents the terminal UPR by inhibiting IRE1α oligomers. Data are plotted as mean ± SD. *p < 0.05 and ** < 0.01.

See also Figure S7.

needed for extra-XBP1 endonucleolytic activation (RIDD); thus, lower concentrations of IRE1α type II kinase inhibitors block RIDD while maintaining XBP1 splicing (Figure 5D). Subsequent work is necessary to understand the consequences of long-term IRE1α inhibition. Although further medicinal chemistry to optimize KIRA6 is beyond the scope of this study, such efforts may lead to first-in-class agents capable of preventing cell loss and affording therapeutic benefit in myriad human

degenerative diseases, including retinitis pigmentosa and diabetes.

## EXPERIMENTAL PROCEDURES

### Tissue Culture, ER Stress Agents, and Small Molecules

Generation of isogenic, stable INS-1 lines was described previously (Han et al., 2009) (see also Extended Experimental Procedures). Thapsigargin (Tg), Brefeldin A (BFA), and Dox were purchased from Sigma-Aldrich. Tunicamycin (Tm) was purchased from Millipore. APY29, KIRA6, (NMe)KIRA6 1NM-PP1, and STF-083010 were synthesized in house (see Extended Experimental Procedures for synthesis, purification, and purity determination methods of small molecules).

### Western Blots and Antibodies

For protein analysis, cells were lysed in M-PER buffer (Thermo Scientific) plus complete EDTA-free protease inhibitor (Roche) and phosphatase inhibitor cocktail (Sigma). Protein concentration was determined using BCA Protein Assay (Thermo). Western blots were performed using 10% and 12% Bis-Tris precast gels (NuPage) on Invitrogen XCell SureLock Mini-Cell modules. Gels were run using MES buffer and transferred onto nitrocellulose transfer membrane using an XCell II Blot Module. Antibody binding was detected by using near-infrared-dye-conjugated secondary antibodies (Li-Cor) on the LI-COR Odyssey scanner or visualized by capturing on a CL-XPosure film using ECL SuperSignal West Dura Extended Duration Substrate (both from Thermo Scientific). See Extended Experimental Procedures for details of the antibodies used.

### RNA Isolation, Quantitative Real-Time PCR, and Primers

RNA was isolated from whole cells using either QIAGEN RNeasy kits or Trizol (Invitrogen). TissueLyser II (QIAGEN) was used for RNA isolation from liver and retina. For standard mRNA detection, generally 1 μg total RNA was reverse transcribed using the QuantiTect Reverse Transcription Kit (QIAGEN). For Q-PCR, we used SYBR green (QIAGEN) and StepOnePlus Real-Time PCR System (Applied Biosystems). Gene expression levels were normalized to GAPDH or Actin. See Extended Experimental Procedures for primer sequences used for Q-PCRs and for details of XBP1 mRNA splicing.

### In Vitro IRE1α* Crosslinking, RNase, and Kinase Assays

See Wang et al. (2012) and the Extended Experimental Procedures for details of RNase, kinase, and oligomerization assays.

### Flow Cytometry

For assaying apoptosis by Annexin V staining, cells were plated in 12-well plates overnight. Cells were then treated with various ER stress agents for indicated times. On the day of analysis, cells were trypsinized and washed in PBS and resuspended in Annexin V binding buffer with Annexin-V FITC (BD PharMingen). Flow cytometry was performed on a Becton Dickinson LSRII flow cytometer.

### Islet Staining

Islets were extracted from C57BL/6 mice using previously reported methods (Szot et al., 2007). Approximately 150 islets were cultured for each condition in triplicate. Nondiabetic human islets were obtained from Prodo Labs (Irvine) and cultured in Prodo Islet Medium (PIM from Prodo Labs). Islets were stained with TUNEL using ApopTag Red In Situ Apoptosis Detection Kit (Millipore) according to the manufacturer's instructions. Islets were also costained with anti-TXNIP (MBL International), guinea pig anti-insulin (Zymed), DAPI (Sigma), and goat anti-guinea pig secondary (Rockland) before mounting onto slides with VectaShield (Vector Laboratories). At least 10 islets and >500 β cell nuclei were counted per group, in triplicate. See also Extended Experimental Procedures for details of fixation and staining.

### Intravitreal Injections of Small Molecules

2 μl was injected intravitreally into each eye to achieve indicated final concentrations based on known rat vitreous volumes. Tm (20 μg/μl final) ± KIRA6 (10 μM final) was injected into SD rats at P21 with equivalent DMSO as vehicle control. Retinas were collected at 72 and 96 hr after injections in Trizol (Invitrogen) for qPCR. Eyes were examined by optical coherence tomography (OCT) 7 days postinjection and then collected for morphological analysis. P23H rats were injected with KIRA6 (10 μM final) or DMSO vehicle at P9 and P15, and eyes were examined at P40 by OCT and by morphological analysis. See Extended Experimental Procedures for details of image guided (OCT), morphological analysis, and electroretinography (ERG).

### Mouse Systemic Injections

Male *Ins2*$^{+/Akita}$ mice were injected i.p. with KIRA6 in a 2 mg/ml solution made of 3% ethanol: 7% Tween-80: 90% saline twice a day (b.i.d.). Same solution without KIRA6 is denoted as vehicle. C567BL/6 mice were also injected with the same KIRA6 solution and indicated doses of Tm for liver analysis. See Extended Experimental Procedures for details of islet explant experiments, GSIS, proliferation studies, blood glucose determination, glucose tolerance tests, insulin and C-peptide measurements, and β cell area determination.

## SUPPLEMENTAL INFORMATION

Supplemental Information includes Extended Experimental Procedures, seven figures, and seven movies and can be found with this article online at http://dx.doi.org/10.1016/j.cell.2014.07.002.

## AUTHOR CONTRIBUTIONS

R.G., L.W., E.S.W., D.J.M., S.A.O., and F.R.P designed the experiments. R.G., L.W., K.P., D.C., A.I., S.M., K.F.W., S.B.H., A.K.M., and E.L.S. performed in vitro and cell culture experiments. R.G., M.T., S.M., H.M., and F.R.P. performed ex vivo and in vivo pancreas and liver experiments. E.S.W., R.G., and M.V.A. performed retina experiments. B.G.K.P., S.B.H., A.K.M., M.J.G., B.J.B., and D.J.M designed and synthesized KIRA6. B.B. and S.C.S. computationally modeled KIRAs. E.L.S., D.B.G., M.S.G., B.J.B., D.J.M., S.A.O., and F.R.P. analyzed all data. With all authors' comments, S.A.O. and F.R.P. wrote the manuscript. R.G., L.W., E.S.W., D.J.M., S.A.O., and F.R.P edited the manuscript.

## ACKNOWLEDGMENTS

We thank Michael Matthes and Doug Yasumura for technical assistance with rat models, Vinh Nguyen for islet isolation, and Oakes and Papa lab members for discussions. The work was supported by National Institutes of Health grants DP2OD001925 (F.R.P.), RO1 CA136577 (S.A.O.), RO1 DK080955 (F.R.P.), RO1 DK095306 (S.A.O. and F.R.P.), RO1 DK100623 (D.J.M. and F.R.P.), PO1 HL108794 (F.R.P.), P30 DK063720 (F.R.P. and M.S.G.), UO1 DK089541 (F.R.P. and M.S.G.), RO1 DK021344 (M.S.G.), RO1 GM086858 (D.J.M.), R21 CA177402 (D.J.M.), EY019504 (D.B.G.), EY01919 (D.B.G.), EY06842 (D.B.G.), and F31-NS083323 (E.S.W.); HHMI Physician-Scientist Early Career Award (S.A.O.); American Cancer Society Research Scholar Award (S.A.O.); Burroughs Wellcome Foundation (F.R.P.); Juvenile Diabetes Research Foundation (F.R.P. and S.A.O.); Harrington Discovery Institute Scholar-Innovator Award (S.A.O. and F.R.P.); Alfred P. Sloan Foundation (D.J.M.); Camille and Henry Dreyfus Foundation (D.J.M.); National Science Foundation (E.S.W.); and American Diabetes Association ADA-7-07-MN-22 (H.M.S.).

Received: March 23, 2014
Revised: June 9, 2014
Accepted: July 1, 2014
Published: July 10, 2014

## REFERENCES

Ali, M.M., Bagratuni, T., Davenport, E.L., Nowak, P.R., Silva-Santisteban, M.C., Hardcastle, A., McAndrews, C., Rowlands, M.G., Morgan, G.J., Aherne, W., et al. (2011). Structure of the Ire1 autophosphorylation complex and implications for the unfolded protein response. EMBO J. *30*, 894–905.

Calfon, M., Zeng, H., Urano, F., Till, J.H., Hubbard, S.R., Harding, H.P., Clark, S.G., and Ron, D. (2002). IRE1 couples endoplasmic reticulum load to secretory capacity by processing the XBP-1 mRNA. Nature *415*, 92–96.

Cox, J.S., and Walter, P. (1996). A novel mechanism for regulating activity of a transcription factor that controls the unfolded protein response. Cell *87*, 391–404.

Credle, J.J., Finer-Moore, J.S., Papa, F.R., Stroud, R.M., and Walter, P. (2005). On the mechanism of sensing unfolded protein in the endoplasmic reticulum. Proc. Natl. Acad. Sci. USA *102*, 18773–18784.

Festjens, N., Vanden Berghe, T., Cornelis, S., and Vandenabeele, P. (2007). RIP1, a kinase on the crossroads of a cell's decision to live or die. Cell Death Differ. *14*, 400–410.

Gorbatyuk, M.S., Knox, T., LaVail, M.M., Gorbatyuk, O.S., Noorwez, S.M., Hauswirth, W.W., Lin, J.H., Muzyczka, N., and Lewin, A.S. (2010). Restoration of visual function in P23H rhodopsin transgenic rats by gene delivery of BiP/Grp78. Proc. Natl. Acad. Sci. USA *107*, 5961–5966.

Greenman, C., Stephens, P., Smith, R., Dalgliesh, G.L., Hunter, C., Bignell, G., Davies, H., Teague, J., Butler, A., Stevens, C., et al. (2007). Patterns of somatic mutation in human cancer genomes. Nature *446*, 153–158.

Han, D., Upton, J.P., Hagen, A., Callahan, J., Oakes, S.A., and Papa, F.R. (2008). A kinase inhibitor activates the IRE1alpha RNase to confer cytoprotection against ER stress. Biochem. Biophys. Res. Commun. *365*, 777–783.

Han, D., Lerner, A.G., Vande Walle, L., Upton, J.P., Xu, W., Hagen, A., Backes, B.J., Oakes, S.A., and Papa, F.R. (2009). IRE1alpha kinase activation modes control alternate endoribonuclease outputs to determine divergent cell fates. Cell *138*, 562–575.

Harding, H.P., Novoa, I., Zhang, Y., Zeng, H., Wek, R., Schapira, M., and Ron, D. (2000). Regulated translation initiation controls stress-induced gene expression in mammalian cells. Mol. Cell *6*, 1099–1108.

Hollien, J., and Weissman, J.S. (2006). Decay of endoplasmic reticulum-localized mRNAs during the unfolded protein response. Science *313*, 104–107.

Hollien, J., Lin, J.H., Li, H., Stevens, N., Walter, P., and Weissman, J.S. (2009). Regulated Ire1-dependent decay of messenger RNAs in mammalian cells. J. Cell Biol. *186*, 323–331.

Kohno, K. (2007). How transmembrane proteins sense endoplasmic reticulum stress. Antioxid. Redox Signal. *9*, 2295–2303.

Korennykh, A.V., Egea, P.F., Korostelev, A.A., Finer-Moore, J., Zhang, C., Shokat, K.M., Stroud, R.M., and Walter, P. (2009). The unfolded protein response signals through high-order assembly of Ire1. Nature *457*, 687–693.

Lee, A.H., Iwakoshi, N.N., and Glimcher, L.H. (2003). XBP-1 regulates a subset of endoplasmic reticulum resident chaperone genes in the unfolded protein response. Mol. Cell. Biol. *23*, 7448–7459.

Lerner, A.G., Upton, J.P., Praveen, P.V., Ghosh, R., Nakagawa, Y., Igbaria, A., Shen, S., Nguyen, V., Backes, B.J., Heiman, M., et al. (2012). IRE1$\alpha$ induces thioredoxin-interacting protein to activate the NLRP3 inflammasome and promote programmed cell death under irremediable ER stress. Cell Metab. *16*, 250–264.

Li, H., Korennykh, A.V., Behrman, S.L., and Walter, P. (2010). Mammalian endoplasmic reticulum stress sensor IRE1 signals by dynamic clustering. Proc. Natl. Acad. Sci. USA *107*, 16113–16118.

Lin, J.H., Li, H., Yasumura, D., Cohen, H.R., Zhang, C., Panning, B., Shokat, K.M., Lavail, M.M., and Walter, P. (2007). IRE1 signaling affects cell fate during the unfolded protein response. Science *318*, 944–949.

Lin, J.H., Li, H., Zhang, Y., Ron, D., and Walter, P. (2009). Divergent effects of PERK and IRE1 signaling on cell viability. PLoS ONE *4*, e4170.

Lu, P.D., Jousse, C., Marciniak, S.J., Zhang, Y., Novoa, I., Scheuner, D., Kaufman, R.J., Ron, D., and Harding, H.P. (2004). Cytoprotection by pre-emptive conditional phosphorylation of translation initiation factor 2. EMBO J. *23*, 169–179.

Ofengeim, D., and Yuan, J. (2013). Regulation of RIP1 kinase signalling at the crossroads of inflammation and cell death. Nat. Rev. Mol. Cell Biol. *14*, 727–736.

Papandreou, I., Denko, N.C., Olson, M., Van Melckebeke, H., Lust, S., Tam, A., Solow-Cordero, D.E., Bouley, D.M., Offner, F., Niwa, M., and Koong, A.C. (2011). Identification of an Ire1alpha endonuclease specific inhibitor with cytotoxic activity against human multiple myeloma. Blood *117*, 1311–1314.

Pennesi, M.E., Nishikawa, S., Matthes, M.T., Yasumura, D., and LaVail, M.M. (2008). The relationship of photoreceptor degeneration to retinal vascular development and loss in mutant rhodopsin transgenic and RCS rats. Exp. Eye Res. *87*, 561–570.

Reimold, A.M., Iwakoshi, N.N., Manis, J., Vallabhajosyula, P., Szomolanyi-Tsuda, E., Gravallese, E.M., Friend, D., Grusby, M.J., Alt, F., and Glimcher, L.H. (2001). Plasma cell differentiation requires the transcription factor XBP-1. Nature *412*, 300–307.

Schroder, K., Zhou, R., and Tschopp, J. (2010). The NLRP3 inflammasome: a sensor for metabolic danger? Science *327*, 296–300.

Shimazawa, M., Inokuchi, Y., Ito, Y., Murata, H., Aihara, M., Miura, M., Araie, M., and Hara, H. (2007). Involvement of ER stress in retinal cell death. Mol. Vis. *13*, 578–587.

Shore, G.C., Papa, F.R., and Oakes, S.A. (2011). Signaling cell death from the endoplasmic reticulum stress response. Curr. Opin. Cell Biol. *23*, 143–149.

Szot, G.L., Koudria, P., and Bluestone, J.A. (2007). Murine pancreatic islet isolation. J. Vis. Exp. *2007*, 255.

Tirasophon, W., Welihinda, A.A., and Kaufman, R.J. (1998). A stress response pathway from the endoplasmic reticulum to the nucleus requires a novel bifunctional protein kinase/endoribonuclease (Ire1p) in mammalian cells. Genes Dev. *12*, 1812–1824.

Travers, K.J., Patil, C.K., Wodicka, L., Lockhart, D.J., Weissman, J.S., and Walter, P. (2000). Functional and genomic analyses reveal an essential coordination between the unfolded protein response and ER-associated degradation. Cell *101*, 249–258.

Upton, J.P., Wang, L., Han, D., Wang, E.S., Huskey, N.E., Lim, L., Truitt, M., McManus, M.T., Ruggero, D., Goga, A., et al. (2012). IRE1$\alpha$ cleaves select microRNAs during ER stress to derepress translation of proapoptotic Caspase-2. Science *338*, 818–822.

Urano, F., Wang, X., Bertolotti, A., Zhang, Y., Chung, P., Harding, H.P., and Ron, D. (2000). Coupling of stress in the ER to activation of JNK protein kinases by transmembrane protein kinase IRE1. Science *287*, 664–666.

Wang, L., Perera, B.G., Hari, S.B., Bhhatarai, B., Backes, B.J., Seeliger, M.A., Schürer, S.C., Oakes, S.A., Papa, F.R., and Maly, D.J. (2012). Divergent allosteric control of the IRE1$\alpha$ endoribonuclease using kinase inhibitors. Nat. Chem. Biol. *8*, 982–989.

Xue, Z., He, Y., Ye, K., Gu, Z., Mao, Y., and Qi, L. (2011). A conserved structural determinant located at the interdomain region of mammalian inositol-requiring enzyme 1alpha. J. Biol. Chem. *286*, 30859–30866.

Yoshida, H., Matsui, T., Yamamoto, A., Okada, T., and Mori, K. (2001). XBP1 mRNA is induced by ATF6 and spliced by IRE1 in response to ER stress to produce a highly active transcription factor. Cell *107*, 881–891.

Zhang, K., Wong, H.N., Song, B., Miller, C.N., Scheuner, D., and Kaufman, R.J. (2005). The unfolded protein response sensor IRE1alpha is required at 2 distinct steps in B cell lymphopoiesis. J. Clin. Invest. *115*, 268–281.

Zhang, S.X., Sanders, E., Fliesler, S.J., and Wang, J.J. (2014). Endoplasmic reticulum stress and the unfolded protein responses in retinal degeneration. Exp. Eye Res. *125C*, 30–40.

Zhou, J., Liu, C.Y., Back, S.H., Clark, R.L., Peisach, D., Xu, Z., and Kaufman, R.J. (2006). The crystal structure of human IRE1 luminal domain reveals a conserved dimerization interface required for activation of the unfolded protein response. Proc. Natl. Acad. Sci. USA *103*, 14343–14348.